Electronic Supplementary Material (ESI) for Analyst.

A new and highly efficient CuMOF-based nanoenzyme and its applications for aptamer SERS/FL/RRS/Abs quadruple-mode analysis of ultratrace malachite green

Shuxin Chen, Yue Liu, Zhiyu Qin, Guiqing Wen*, Zhiliang Jiang*

Key Laboratory of Ecology of Rare and Endangered Species and Environmental Protection (Guangxi Normal University), Ministry of Education, Guilin 541004, China; Guangxi Key Laboratory of Environmental Pollution Control Theory and Technology for Science and Education Combined with Science and Technology Innovation Base, Guilin 541004, China.
Correspondence: gqwen@mailbox.gxnu.edu.cn; zljiang@mailbox.gxnu.edu.cn

1. Preparation of MOF and CuNM

CuMOF: Homophthalic acid (1.0 g) was dissolved in 30 mL of methanol/water (1:1) to obtain solution A. $CuSO_4 \cdot 5H_2O$ (2.0 g) was dissolved in 15 mL of H_2O to obtain solution B. B was slowly added to A, and then stirred for 2h, washed 3 times with ethanol and dried at 60 ℃.

TiMOF: Weigh 0.562 g of 2-aminoterephthalic acid(NH_2-BDC) and 0.314 mL of glacial acetic acid dissolved in 40 mL of DMF-methanol (V=9:1), then add 0.592 mL of titanium isopropoxide and disperse by sonication for 30 min. The reaction was carried out in an oven at 150 ℃ for 24 h. Finally, the reaction products were washed with DMF and methanol and then dried at 60 ℃.

ZrMOF: 400 mg of 2,2'-bipyridine-5,5'-dicarboxylic acid was weighed and dissolved in 30 mL of DMF, while $ZrCl_4$ (100 mg) was dissolved in 50 mL of DMF. 1 mL of acetic acid was added after mixing the above two and mixed for 10 min for 18 h. Finally, the reaction products were washed with DMF and THF and dried at 60℃.

FeMOF: $FeCl_3 \cdot 6H_2O$ (0.41 g), NH_2-BDC (0.276 g) and DMF (30 mL) were sealed in a 50 mL PTFE bottle and heated at 120 ℃ for 20 h. When cooled to room temperature, brown crystals of

FeMOF were separated from the solution. Finally the reaction products were washed with DMF and ethanol and dried at 60 °C.

CoMOF: Cobalt nitrate (0.186 g), terephthalic acid (0.133 g) and DMF (25 mL) were sealed in a 50 mL PTFE bottle and heated to 120 °C for 12 h. When cooled to room temperature, the purple crystals of CoMOF were separated from the solution. Finally the reaction products were washed with DMF and ethanol and dried at 60 °C.

NiMOF: 0.166 g of terephthalic acid and 0.067 g of nickel chloride hexahydrate were weighed, dissolved in 20 mL of DMF and completely dissolved by stirring at room temperature. Then 2 mL of 0.4 M sodium hydroxide was slowly added dropwise and the reaction was carried out at 100 °C for 8 h. Finally the reaction products were washed with DMF and ethanol and dried at 60 °C.

The H_2O_2-TMB system was difficult to react under the conditions of a water bath at 50 ℃. In this work, several MOFs were screened for their catalytic effect on the TMB reaction. Among them, CuMOF, ZrMOF, TiMOF and FeMOF can catalyse the H_2O_2-TMB reaction to produce a light blue TMBox. The fluorescence spectrum was obtained by scanning at volt=350 V, excited slit=emission slit=10 nm and the TMBox showed a fluorescence peak at Ex=270 nm, Em=410 nm. For this nanocatalytic system, in a certain concentration range, the four MOFs mentioned above catalyzed the oxidation of TMB by H_2O_2, and as the concentration of MOF increased, the catalytically generated TMBox increased and eventually showed a strong fluorescence effect. In a word, the fluorescence intensity at this site showed a linear increasing relationship with the concentration of MOF. On the contrary, the concentrations of CoMOF and NiMOF showed a linearly decreasing relationship with the fluorescence intensity at this site, while CeMOF, AgMOF and ZnMOF had no catalytic effect on TMB. And it can be compared by the following figure (Fig.S1a-f), CuMOF has better catalytic effect indeed. And at the same time, compared with precious metal (Ag, Au, Pd, and Pt) MOFs, copper MOFs stood out among many high-performance MOFs due to its low cost, high optical performance, and other factors. Therefore, it is used as a precursor for synthesis of CuNM nanoenzymes.

It shows a comparison of the fluorescence spectra of the three MOF derivatives (CuNM, TiNM and ZrNM) in fig.S1g-i, all with varying degrees of improvement compared to the catalytic effect

of the original MOF. The slope of the linear relationship allows a comparison of the strength of the catalytic effect of the catalysts, the stronger the catalytic effect when the slope is higher. The slope of the catalytic relationship is 3236.5 for CuNM and 1610 for CuMOF. It is obvious that CuNM has the best catalytic effect, so CuNM was chosen as the best catalyst for the subsequent experiments.

Porous Cu_2O/Cu/C carbon-based nanoenzymes (CuNM): Referring to previous methods[1，2] and improving them, the above prepared MOF was prepared by high-temperature pyrolysis by taking 1 g of MOF powder in a quartz boat and placing it in a tube furnace under a nitrogen atmosphere throughout, with a heating rate of 10 ℃/min to 700 ℃ and holding it for 2 h. After cooling to room temperature, the CuNM powder was obtained. Furthermore, the optimum preparation conditions were obtained with a heating time of 2 h and a heating temperature of 700 ℃ (Fig.S2).

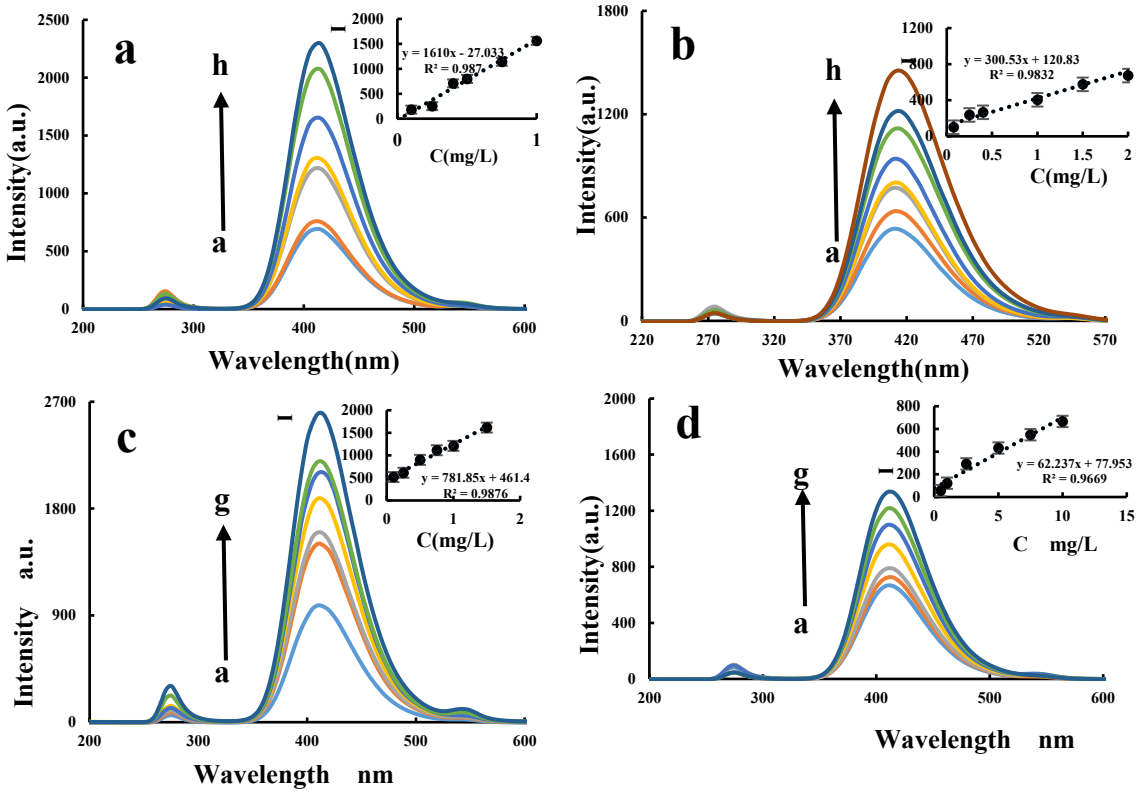

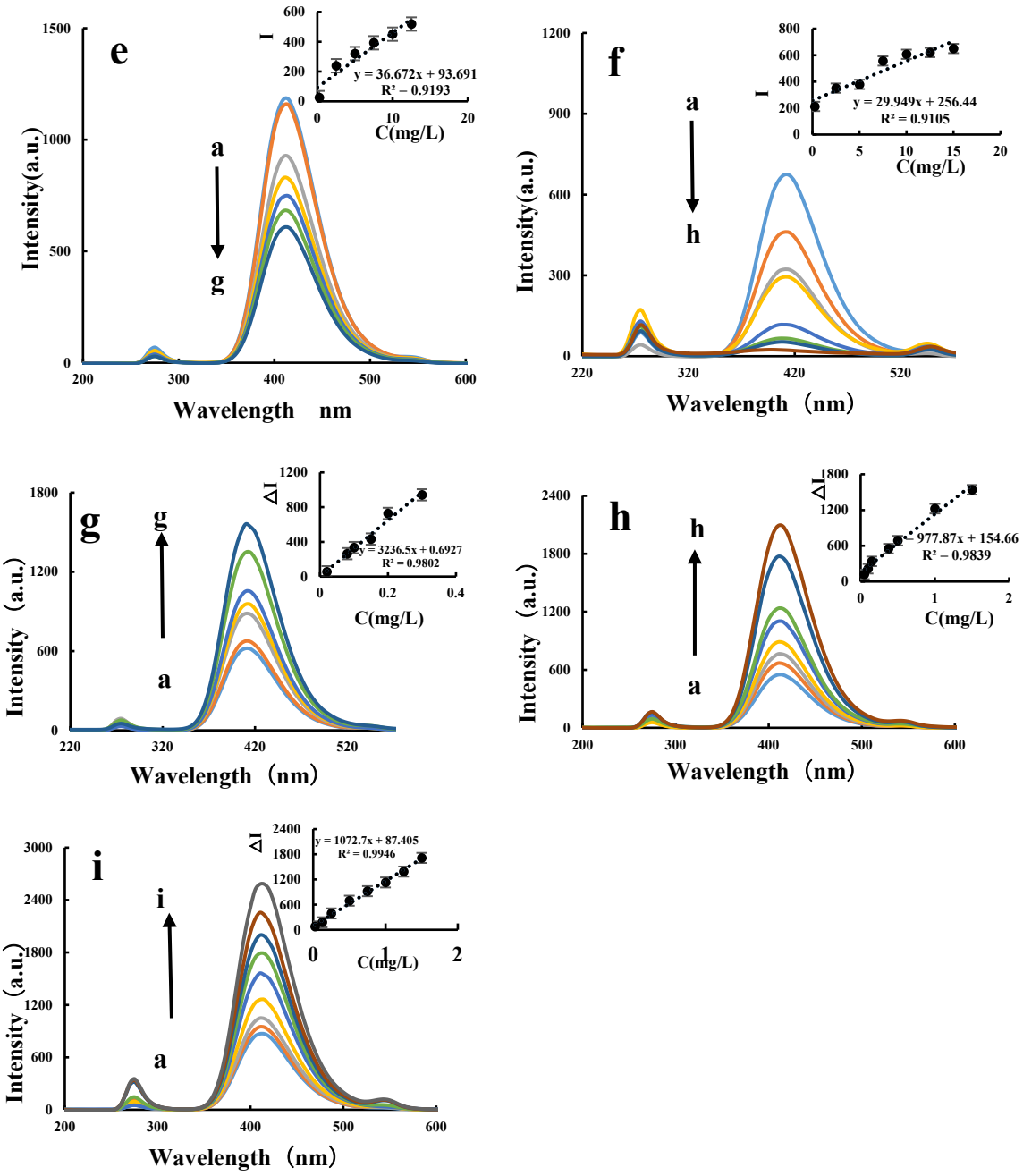

Fig.S1. Fluorescence spectrum of MOF/NM -H_2O_2-TMB-Tris-HCl.

a: a: 0.55mmol/L Tris-HCl +0.025 mmol/L TMB+0.05mmol/L H_2O_2; b: a+0.1mg/L CuMOF; c: a+0.25mg/L CuMOF; d: a+ 0.4mg/L CuMOF; e: a+ 0.5mg/L CuMOF; f: a+ 0.75mg/L CuMOF;g: a+ 1 mg/L CuMOF; h: a+ 1.1mg/L CuMOF.

b:a: 0.55mmol/L PH=4.4 Tris-HCl +0.025 mmol/L TMB+0.05mmol/L H_2O_2; b: a+0.075mg/L TiMOF; c: a+0.25mg/L TiMOF; d: a+ 0.4mg/L TiMOF; e: a+ 1mg/L TiMOF; f: a+ 1.5mg/L TiMOF;g: a+2mg/L TiMOF; h: a+ 2.5mg/L TiMOF.

c:a: 0.55mmol/L PH=4.4 Tris-HCl +0.025 mmol/L TMB+0.05mmol/L H_2O_2; b: a+0.1mg/L ZrMOF;

c: a+0.25mg/L ZrMOF; d: a+ 0.5mg/L ZrMOF; e: a+ 0.75mg/L ZrMOF; f: a+ 1mg/L ZrMOF;g: a+ 1.5mg/L ZrMOF.

d:a: 0.55mmol/L PH=4.4 Tris-HCl +0.025 mmol/L TMB+0.05mmol/L H_2O_2; b: a+0.5mg/L FeMOF; c: a+1mg/L FeMOF; d: a+ 2.5 mg/L FeMOF; e: a+ 5mg/L FeMOF; f: a+ 7.5mg/L FeMOF;g: a+10mg/L FeMOF.

e: a: 0.55mmol/L PH=4.4 Tris-HCl +0.025 mmol/L TMB+0.05mmol/L H_2O_2; b: a+0.25mg/L CoMOF; c: a+2.5mg/L CoMOF; d: a+5 mg/L CoMOF; e: a+ 7.5mg/L CoMOF; f: a+ 10mg/L CoMOF;g: a+12.5mg/L CoMOF.

f: a: 0.55mmol/L PH=4.4 Tris-HCl +0.025 mmol/L TMB+0.05mmol/L H_2O_2; b: a+0.25mg/L NiMOF; c: a+2.5mg/L NiMOF; d: a+ 5mg/L NiMOF; e: a+ 7.5mg/L NiMOF; f: a+ 10mg/L NiMOF; g: a+12.5mg/L NiMOF; h: a+ 15mg/L NiMOF.

g:a: pH 4.4 Tris-HCl+0.025 mmol/L TMB+0.05mmol/L H_2O_2; b: a+0.02mg/L CuNM; c: a+0.08mg/L CuNM; d: a+ 0.1mg/L CuNM; e: a+ 0.15mg/L CuNM; f: a+ 0.2mg/L CuNM;g: a+ 0.3mg/L CuNM.

h: a: 0.55mmol/L PH=4.4 Tris-HCl +0.025 mmol/L TMB+0.05mmol/L H_2O_2; b: a+0.05mg/L TiNM; c: a+0.1mg/L TiNM; d: a+ 0.15mg/L TiNM; e: a+0.375mg/L TiNM; f: a+ 0.5mg/L TiNM;g: a+1mg/L TiNM; h: a+ 1.5mg/L TiNM.

i: a: 0.55mmol/L PH=4.4 Tris-HCl +0.025 mmol/L TMB+0.05mmol/L H_2O_2; b: a+0.025mg/L ZrNM; c: a+0.125mg/L ZrNM; d: a+ 0.25mg/L ZrNM; e: a+0.5mg/L ZrNM; f: a+ 0.75mg/L ZrNM; g: a+1mg/L ZrNM; h: a+ 1.25mg/L ZrNM; i: a+ 1.5mg/L ZrNM.

2. Optimization of CuNM preparation conditions

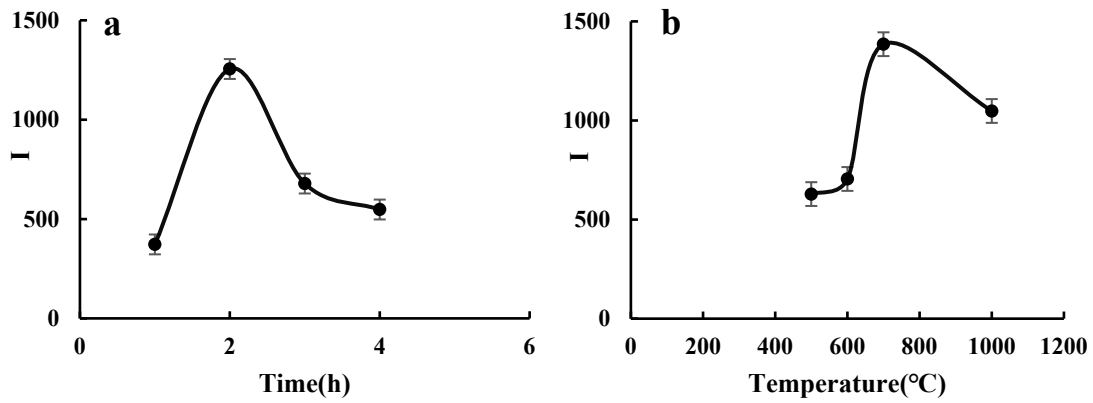

Fig.S2. Optimisation of CuNM preparation conditions

a: Effect of time on the system ΔI; b: Effect of temperature on the system ΔI

3. Characterisation of CuMOF/CuNM

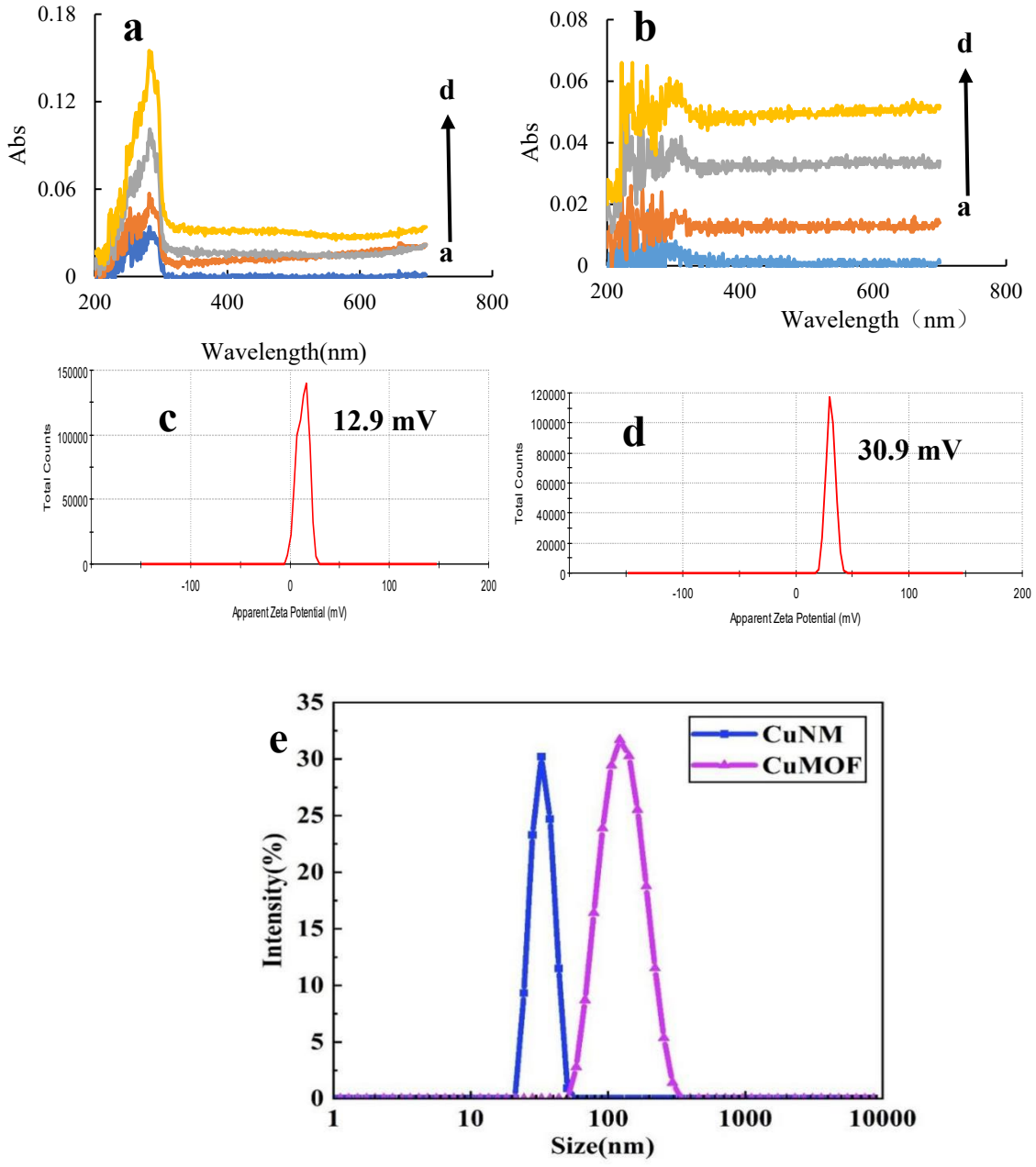

Fig.S3. Abs spectra, potential map and particle size distribution of CuMOF/CuNM

a: Abs spectra of CuMOF，the a-d curves represent 250, 500, 1000, 2000 μg/L CuMOF. b: Abs spectra of CuNM，the a-d curves represent 500, 1000, 1500, 2000 μg/L CuNM;

c、d: Zeta potential diagram of CuMOF/CuNM;

e: Particle size distribution diagram of CuMOF/CuNM.

4. Stability of CuMOF/CuNM and SERS/UV-vis spectroscopy of nanocatalytic systems

The stability of CuNM is beneficial for the development of accurate and reasonable analytical methods. The prepared CuMOF and CuNM solutions were stored in a refrigerator at 4°C. The RRS and Abs signals of CuMOF and CuNM were recorded for 15 consecutive days with RSDs of 5.38% and 2.57%, respectively (Fig.S4a). CuNM shows good stability over time. In addition, the stability of CuMOF and CuNM in 200 mmol/L NaCl solution was studied. The results show that the RRS and Abs signals of CuNM tended to be stable in NaCl solution over time (Fig.S4b-c). The experimental results indicate that the method has good stability.

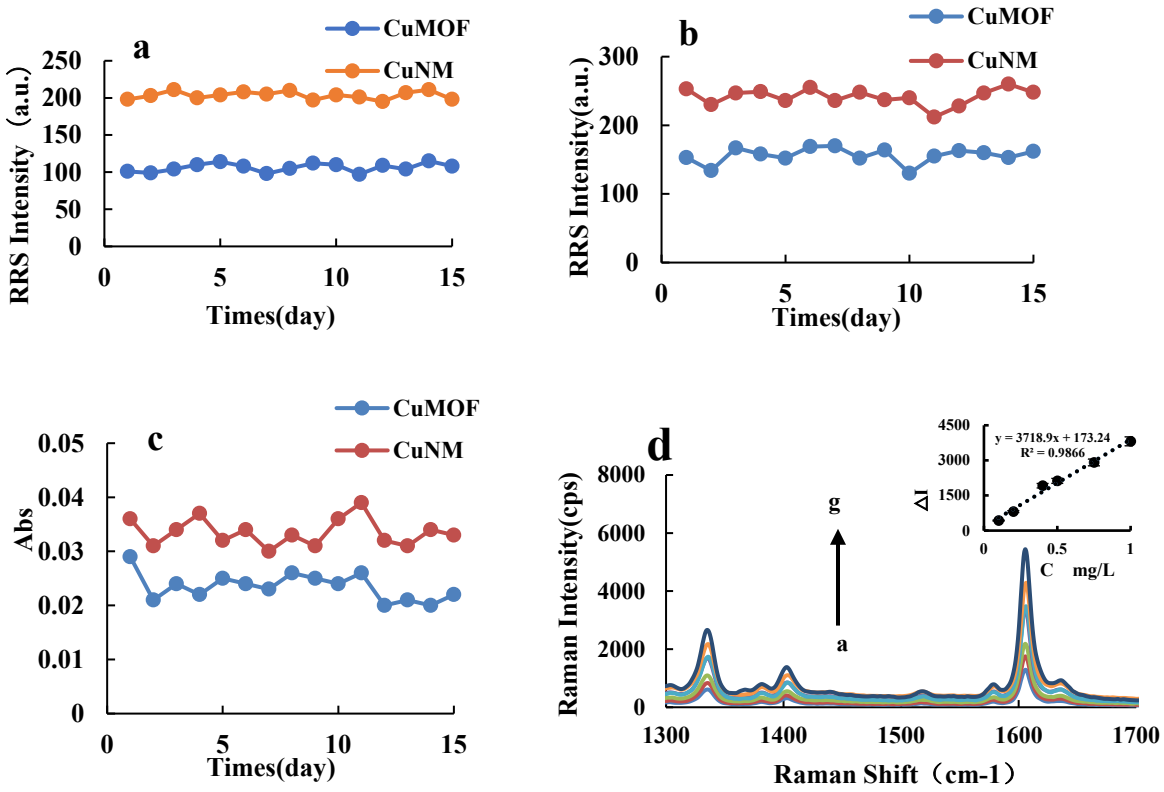

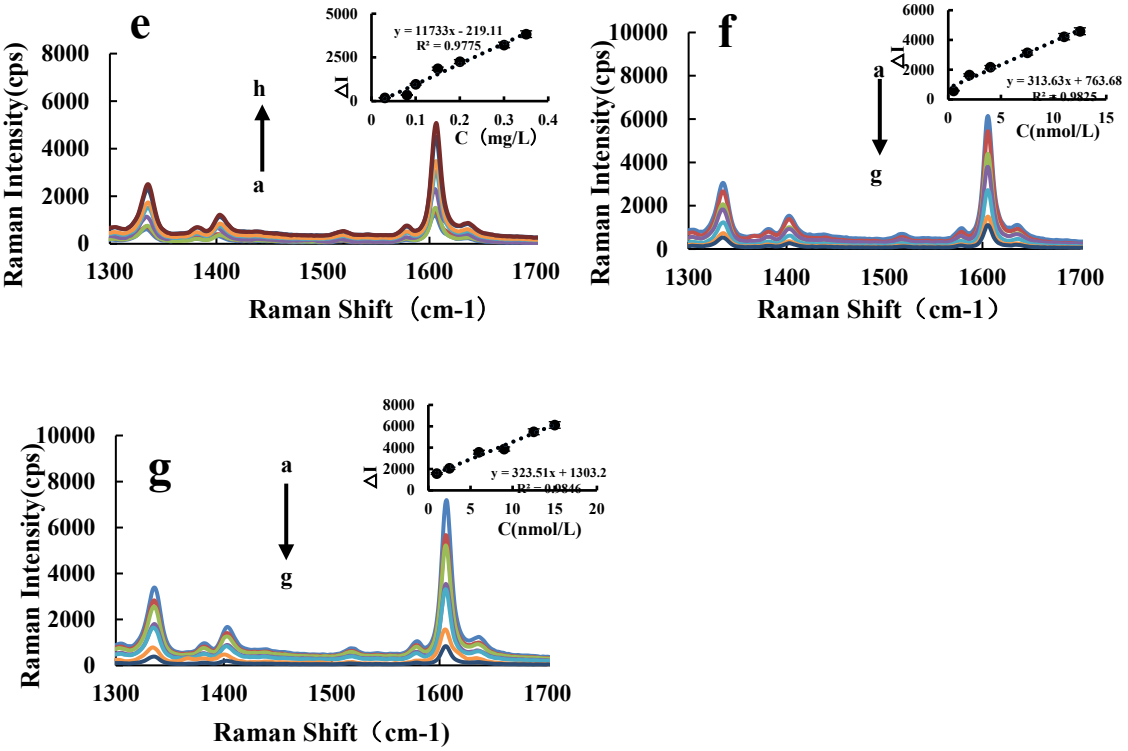

Fig.S4. Stability of CuMOF/CuNM, SERS spectrum of CuMOF/CuNM-H_2O_2-TMB-Tris-HCl system, SERS spectrum of CuMOF/CuNM-H_2O_2-TMB-Tris-HCl-Apt system

a：Stability of CuMOF/CuNM in water;

b：Stability of CuMOF/CuNM in 200 mmol/L NaCl solution (measured by RRS)；

c：Stability of CuMOF/CuNM in 200 mmol/L NaCl solution (measured by Abs);

d：SERS spectrum of CuMOF-H_2O_2-TMB-Tris-HCl system：a: 0.55 mmol/LpH=4.4 Tris-HCl +0.025 mmol/L TMB+0.05mmol/L H_2O_2+11.6 mg/L AgNPs; b: a+0.1 mg/L CuMOF; c: a+0.2 mg/L CuMOF; d: a+ 0.4 mg/L CuMOF; e: a+ 0.5 mg/L CuMOF; f: a+ 0.75 mg/L CuMOF; g: a+ 1 mg/L CuMOF；

e：SERS spectrum of CuNM-H_2O_2-TMB-Tris-HCl system：a: 0.55mmol/L pH=4.4 Tris-HCl+0.025 mmol/L TMB+0.05mmol/L H_2O_2+11.6 mg/L AgNPs; b: a+0.03mg/LCuNM; c: a+0.08mg/LCuNM; d: a+ 0.1mg/LCuNM; e: a+ 0.15mg/LCuNM; f: a+ 0.2mg/LCuNM;g: a+ 0.3mg/LCuNM; h: a+ 0.35mg/LCuNM.

f：SERS spectrum of CuMOF-H_2O_2-TMB-Tris-HCl-Apt system：a: 0.55 pH=4.4 mmol/L Tris-HCl +0.025 mmol/L TMB+0.05mmol/L H_2O_2+0.5 mg/L CuMOF; b: a+0.5nmol/LApt; c: a+2nmol/LApt; d: a+4 nmol/LApt; e: a+7.5nmol/LApt; f: a+ 11nmol/LApt;g: a+ 12.5nmol/LApt.

g： SERS spectrum of CuNM-H_2O_2-TMB-Tris-HCl-Apt system：a: 0.55 pH=4.4 mmol/L Tris-HCl +0.025 mmol/L TMB+0.05mmol/L H_2O_2+0.3 mg/L CuNM; b: a+1nmol/LApt; c: a+2.5nmol/LApt; d: a+6 nmol/LApt; e: a+9nmol/LApt; f: a+ 12.5nmol/LApt; g: a+ 15nmol/LApt.

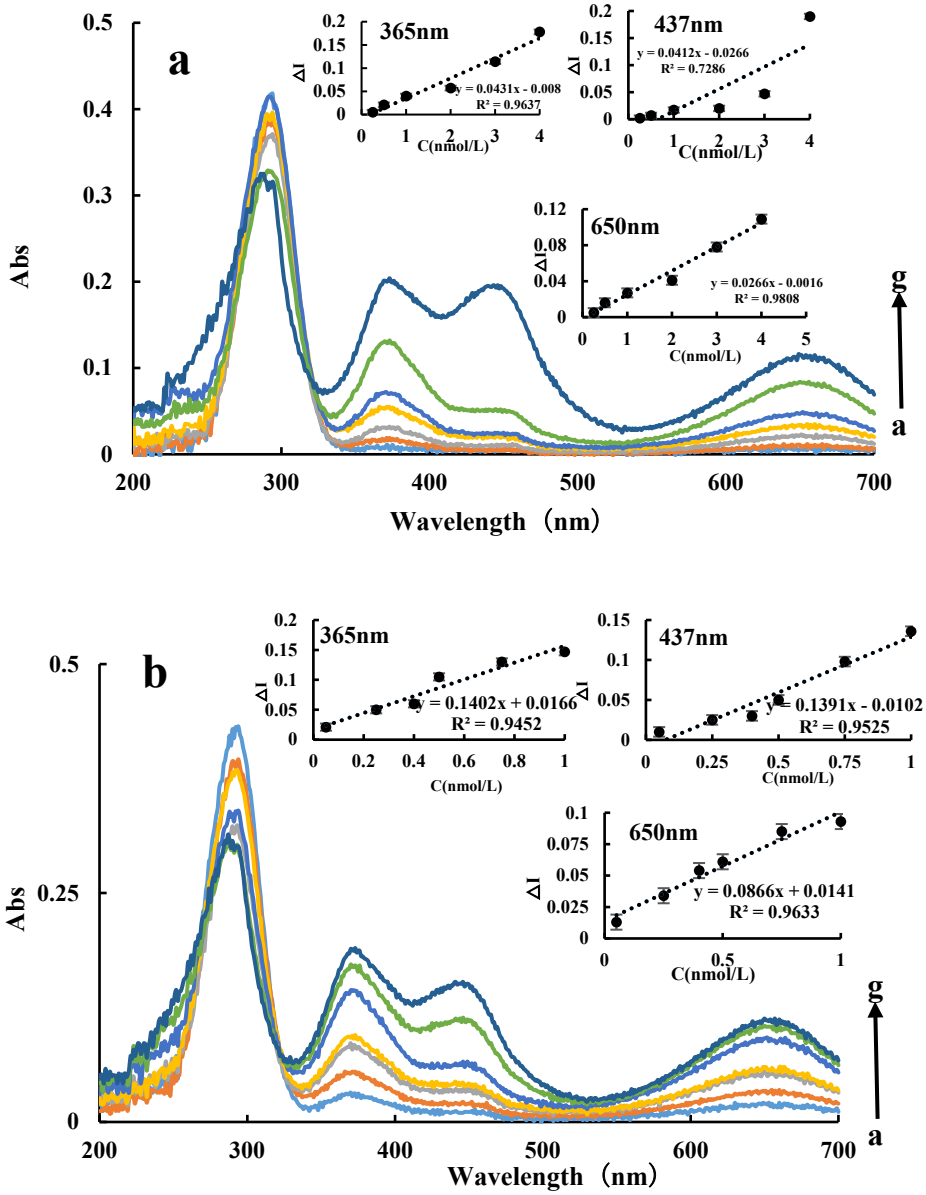

Fig.S5. UV absorption spectra of CuMOF/ CuNM -H_2O_2-TMB-Tris-HCl-Apt-MG system **a:** a: 0.55mmol/L pH=4.4 Tris-HCl +0.0375 mmol/L TMB+0.05mmol/L H_2O_2+0.5 mg/LCuMOF+15nmol/LApt+11.6mg/LAgNPs; b:a+0.25nmol/LMG; c: a+0.5nmol/L MG; d: a+1 nmol/LMG; e: a+2nmol/L MG; f: a+ 3nmol/L MG;g: a+ 4nmol/L MG.

b: a: 0.55mmol/L pH=4.4 Tris-HCl +0.0375 mmol/L TMB+0.05mmol/L H_2O_2+0.3 mg/LCuNM+20nmol/LApt+11.6mg/L AgNPs; b: a+0.05nmol/L MG; c: a+0.25nmol/L MG; d: a+0.4 nmol/LMG; e: a+0.5nmol/LMG; f: a+ 0.75nmol/LMG; g: a+ 1nmol/LMG.

5. Condition optimization

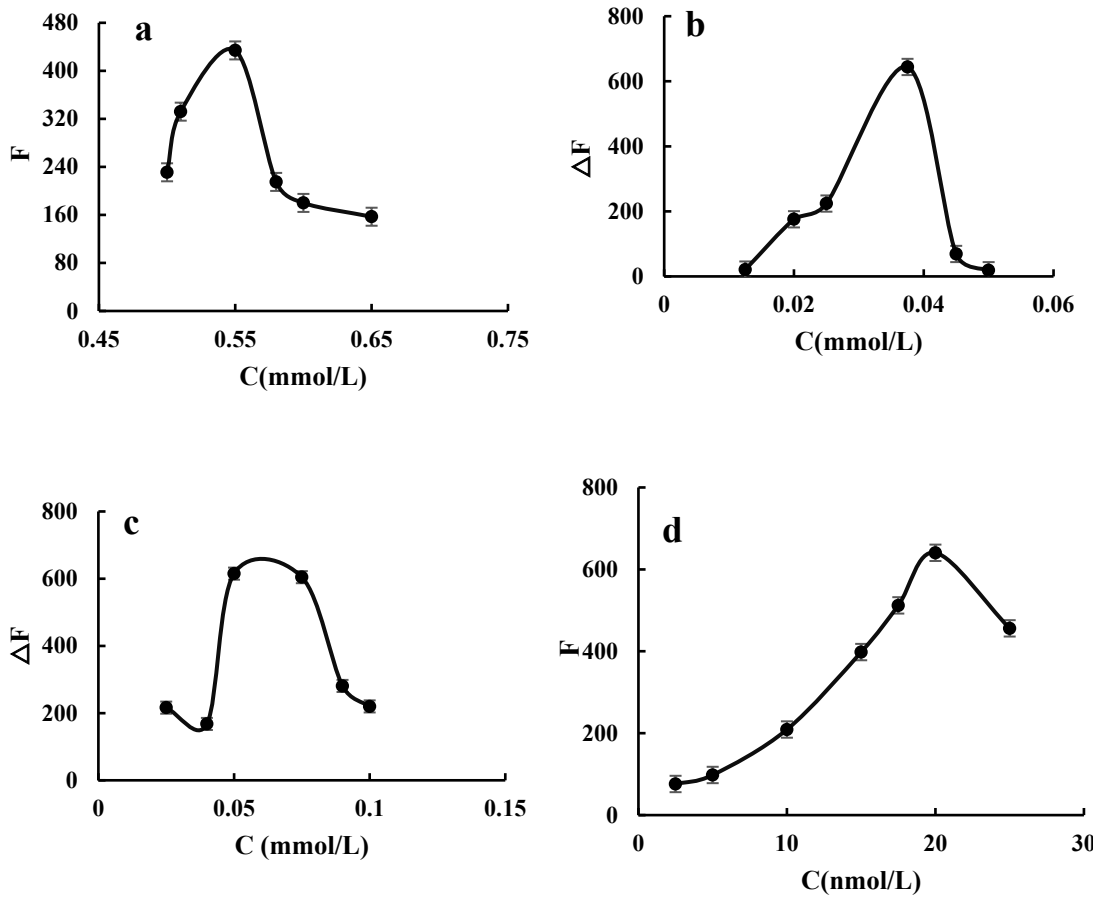

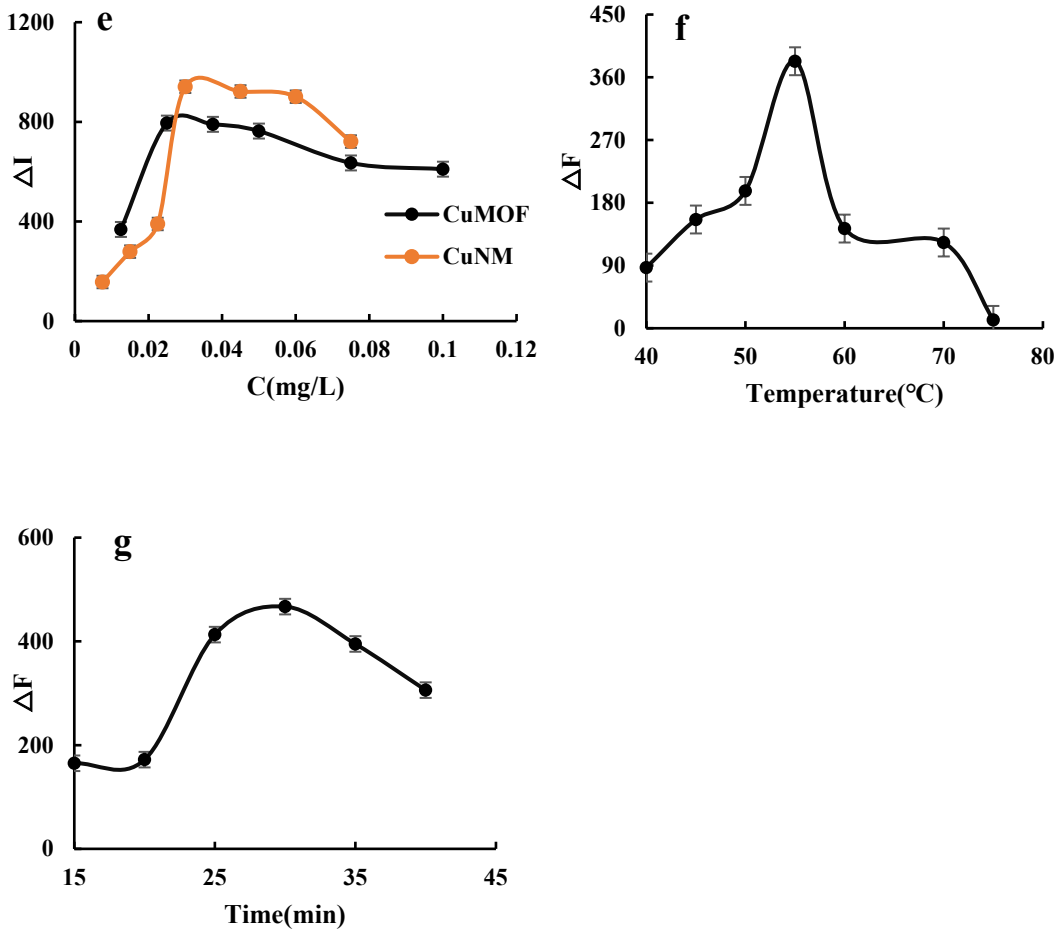

Fig.S6. Optimization of analytical conditions for fluorescent systems

a：**Effect of Tris-HCl buffer solution on system ΔF**，a: 0.03 mg/L CuNM+0.05 mmol/L H_2O_2+ 0.0375mmol/L TMB+ pH=4.4 Tris-HCl+20 nmol/L Apt+0.1nmol/L MG

b: **Effect of TMB concentration on system ΔF**，a: 0.03 mg/L CuNM + 0.05 mmol/L H_2O_2+TMB+ 0.55 mmol/L pH=4.4 Tris-HCl+20 nmol/L Apt +0.1nmol/L MG

c:**Effect of H_2O_2 concentration on system ΔF**，a: 0.03 mg/L CuNM +H_2O_2+ 0.0375mmol/L TMB+ 0.55 mmol/L pH=4.4 Tris-HCl+20 nmol/L Apt +0.1nmol/L MG

d: **Effect of Apt concentration on system ΔF**，a: 0.03 mg/L CuNM + 0.05 mmol/L H_2O_2+ 0.0375 mmol/L TMB+ 0.55 mmol/L pH=4.4 Tris-HCl+ Apt +0.1nmol/L MG

e: **Effect of CuMOF/CuNM concentration on system ΔF**，a: CuMOF/CuNM + 0.05 mmol/L H_2O_2+ 0.0375 mmol/L TMB+ 0.55 mmol/L pH=4.4 Tris-HCl+20 nmol/L Apt +0.1nmol/L MG

f：**Effect of temperature on the system ΔF**，a: 0.03 mg/L CuNM + 0.05 mmol/LH_2O_2+

0.0375mmol/L TMB+ 0.55 mmol/L pH=4.4 Tris-HCl+20 nmol/L Apt +0.1nmol/L MG

g: **Effect of time on the system ΔF**，0.03 mg/L CuNM + 0.05 mmol/LH_2O_2+ 0.0375mmol/L TMB+ 0.55 mmol/L pH=4.4 Tris-HCl+20 nmol/L Apt +0.1nmol/L M

6. Comparison of the nanocatalysis

Table S1 Comparison of NM/HRP-H_2O_2-TMB catalysis with FL technique

Catalysts	Linearity range (mg/L)	Regression equation	Correlation coefficient
CuMOF	0.1-1.1	ΔF_{410nm}=1610C - 27.03	0.987
TiMOF	0.075-2.5	ΔF_{410nm}=300.53C + 120.8	0.9832
ZrMOF	0.1-1.5	ΔF_{410nm}=781.85C + 461.4	0.9876
FeMOF	0.5-10	ΔF_{410nm}=62.24C + 77.95	0.9669
CoMOF	0.25-12.5	ΔF_{410nm}=36.67C + 93.7	0.9193
NiMOF	0.25-15	ΔF_{410nm}=29.95C + 256.4	0.9105
CuNM	0.02-0.3	ΔF_{410nm}= 3236.5 C + 0.69	0.9802
TiNM	0.05-1.5	ΔF_{410nm}= 977.87C + 154.7	0.9839
ZrNM	0.025-1.5	ΔF_{410nm}= 1072.7C + 87.4	0.9946
HRP	0.05-1	ΔF_{410nm}= 1103.7C + 76.96	0.9794

7. Comparison of the characteristics of some of the reported MG analysis methods

Table S2 Comparison of the characteristics of some of the reported MG analysis methods

Analytical methods	Analysis principle	Linear range	LOD	Analysis characteristics	References

Enzyme-linked immunosorbent assay （ELISA）	Direct competitive ELISA was used to detect MG using magnetic molecularly imprinted polymers (MMIPs) as biomimetic antibodies	0.1-10000 μg/L.	0.1 μg/L	This method can quickly detect MG in fish samples with good specificity, accuracy, and reliability	[3]
Visualization of High Performance Liquid Chromatography （HPLC-VIS）	After cleaning with immunoaffinity column (IAC), HPLC was used to determine the residue in fish muscle. And then extracting the residue, the extract was purified on the prepared IAC. Finally, analyze the eluent using HPLC-VIS.	0.5-10 ng/g	0.15 ng/g	High selectivity, sensitivity, and low cost	[4]
Fluorescent sensor	A sensitive fluorescence sensor for detecting MG was prepared by decorating molecular imprinted polymers (MIPs) onto the surface of CdTe quantum dots (QDs).	0.08-20 μmol/L	12 μg/kg	Applied for rapid detection of MG in fish samples	[5]
	Constructed a MG detection ratio fluorescence sensor based on CdTe quantum dots and N, S-GQDs	-	0.4597 nmol/L	Quantitative and visual detection for MG	[6]
Electrochemical method	A highly sensitive voltammetric method has been established for the rapid	0.02–40 nmol/L	4.0 nmol/L	This method has good daily repeatability, stability, and anti-	[7]

	determination of trace amounts of MG in aquaculture and fisheries using an acetylene black paste electrode modified with cetylpyridinium bromide.			interference ability	
Surface Enhanced Raman Scattering(SERS)	SERS active particles were developed by using magnetic nanoparticles (MNPs) as the core, which were uniformly decorated with AuNP and then coated with a MOF shell of MIL-100 (Fe). It acted as a filter, allowing only appropriately sized molecules to approach the internal AuNP, thereby avoiding food matrix interference and improving the recognition ability of the analyte.	-	1.32×10^{-10} mol/L	MG can be detected in shrimp	[8]
	In this method, sea urchin-like Au@SiO2 nanoparticles (SG@SiO2 NPs) were designed and synthesised to improve their stability. The morphology of SG@SiO2 NPs and the thickness of the silica shell layer were	10^{-5}-10^{-9} mol/L	1.5×10^{-9}mol/L	This method can be used for micro detection of MG in actual samples	[9]

	adjusted, resulting in good SERS performance.				
SERS/RRS/FL/Abs	Aptamer-mediated CuNM-catalyzed oxidation of TMB for detection of MG.	0.004-1 nmol/L	0.0032 nmol/L	Low detection limits, stable, sensitive, simple to operate, low cost, good specificity	This work

8. Influence of interfering ions

Table S3 Influence of interfering ions on FL determination of MG

Coexistence of material	Relative ratio	Relative error（%）	Coexistence of material	Relative ratio	Relative error（%）
Al^{3+}	500	7.6	Mg^{2+}	1000	-5.8
Co^{2+}	1000	1.0	CH_3COO^-	200	-6.1
Mn^{2+}	1000	4.6	SO_4^{2-}	1000	-0.1
NO_3^-	200	7.1	Ni^{2+}	1000	3.4
Ba^{2+}	1000	3.9	HCO_3^-	200	-2.9
K^+	1000	0.3	CO_3^{2-}	1000	0.1
CV	100	-1.9	I^-	1000	-2.6
NO_2^-	500	0.5	Ca^{2+}	1000	1.8
NH_4^+	1000	8.4	MB	50	3.5
Zn^{2+}	500	7.0	RBG	10	3.4
Hydathion	500	-6.5	SO_4^{2-}	1000	-0.1
Tetracycline	200	0.3	Malathion	500	-0.3
Oxytetracycline	200	-1.8			

References

[1] J. Li, L. Huang, X. Jiang, L. Zhang, X. Sun, Preparation and characterization of ternary Cu/Cu2O/C composite: An extraordinary adsorbent for removing anionic organic dyes from water, Chem. Eng. J. 404 (2021) 127091. https://doi.org/10.1016/j.cej.2020.127091.

[2] T. Liu, R. Hu, X. Zhang, K. Zhang, Y. Liu, X. Zhang, R.-Y. Bai, D. Li, Y.-H. Yang, Metal–organic framework nanomaterials as novel signal probes for electron transfer mediated ultrasensitive electrochemical immunoassay, Anal Chem 88 (2016) 12516-12523. https://doi.org/10.1021/acs.analchem.6b04191.

[3] L. Li, Z.Z. Lin, A.H. Peng, H.P. Zhong, X.M. Chen, Z.Y. Huang, Biomimetic ELISA detection of malachite green based on magnetic molecularly imprinted polymers, J Chromatogr B Analyt Technol Biomed Life Sci 1035 (2016) 25-30. http://dx.doi.org/10.1016/j.jchromb.2016.09.015.

[4] J. Xie, T. Peng, D.D. Chen, Q.J. Zhang, G.M. Wang, X. Wang, Q. Guo, F. Jiang, D. Chen, J. Deng, Determination of malachite green, crystal violet and their leuco-metabolites in fish by HPLC-VIS detection after immunoaffinity column clean-up, J Chromatogr B Analyt Technol Biomed Life Sci 913-914 (2013) 123-128. http://dx.doi.org/10.1016/j.jchromb.2012.12.002.

[5] X. Cai, F. Ma, J. Jiang, X. Yang, Z. Zhang, Z. Jian, M. Liang, P. Li, L. Yu, Fe-N-C single-atom nanozyme for ultrasensitive, on-site and multiplex detection of mycotoxins using lateral flow immunoassay, J Hazard Mater 441 (2022) 129853. https://doi.org/10.1016/j.jhazmat.2022.129853.

[6] J. Qiu, L. Na, Y. Li, W. Bai, J. Zhang, L. Jin, N,S-GQDs mixed with CdTe quantum dots for ratiometric fluorescence visual detection and quantitative analysis of malachite green in fish, Food Chem 390 (2022) 133156. https://doi.org/10.1016/j.foodchem.2022.133156.

[7] P. Deng, J. Feng, Y. Wei, J. Xiao, J. Li, Q. He, Fast and ultrasensitive trace malachite green detection in aquaculture and fisheries by using hexadecylpyridinium bromide modified electrochemical sensor, J FOOD COMPOS ANAL 102 (2021) 104003. https://doi.org/10.1016/j.jfca.2021.104003.

[8] H. Pu, H. Zhu, F. Xu, D.W. Sun, Development of core-satellite-shell structured MNP@Au@MIL-100(Fe) substrates for surface-enhanced Raman spectroscopy and their applications in trace level determination of malachite green in prawn, J Raman Spectrosc 53 (2022) 682-693.https://doi.org/10.1002/jrs.6293.

[9] Y. Liu, L. Lei, Y. Wu, Y. Chen, J. Yan, W. Zhu, X. Tan, Q. Wang, Fabrication of sea urchin-like Au@SiO2 nanoparticles SERS substrate for the determination of malachite green in tilapia, VIB SPECTROSC 118 (2022) 103319. https://doi.org/10.1016/j.vibspec.2021.103319.